Supplement of Clim. Past, 17, 2559–2576, 2021
https://doi.org/10.5194/cp-17-2559-2021-supplement

Climate of the Past
Open Access

Supplement of

A new perspective on permafrost boundaries in France during the Last Glacial Maximum

Kim H. Stadelmaier et al.

Correspondence to: Kim H. Stadelmaier (kim.stadelmaier@kit.edu)

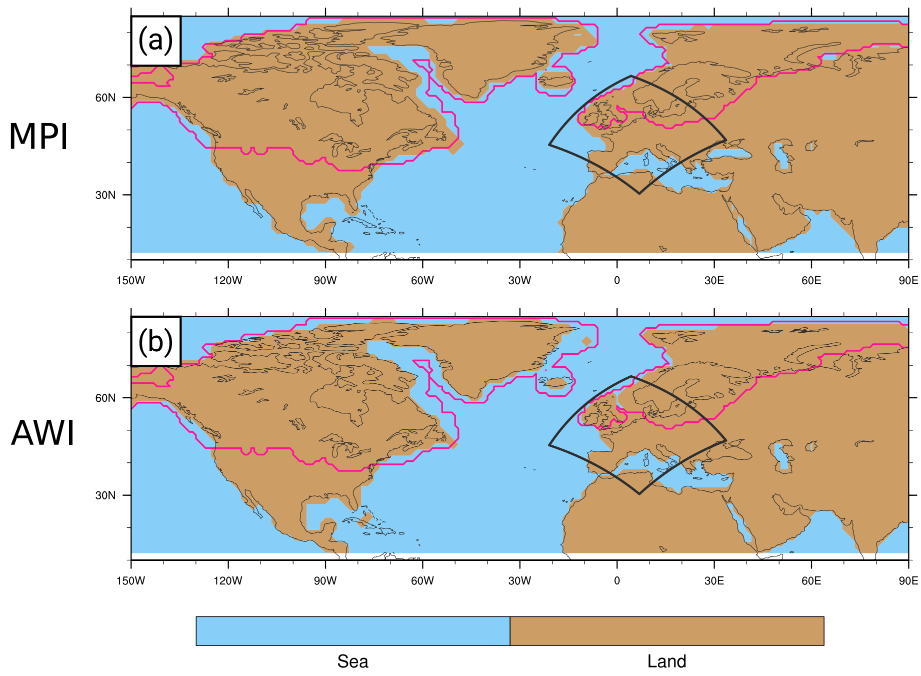

Figure S1. GCM land and sea distribution of the MPI *(a)* and the AWI simulation *(b)*. Thick black line: WRF Domain 1, thin black line: LGM coastline, pink line: LGM ice sheet.

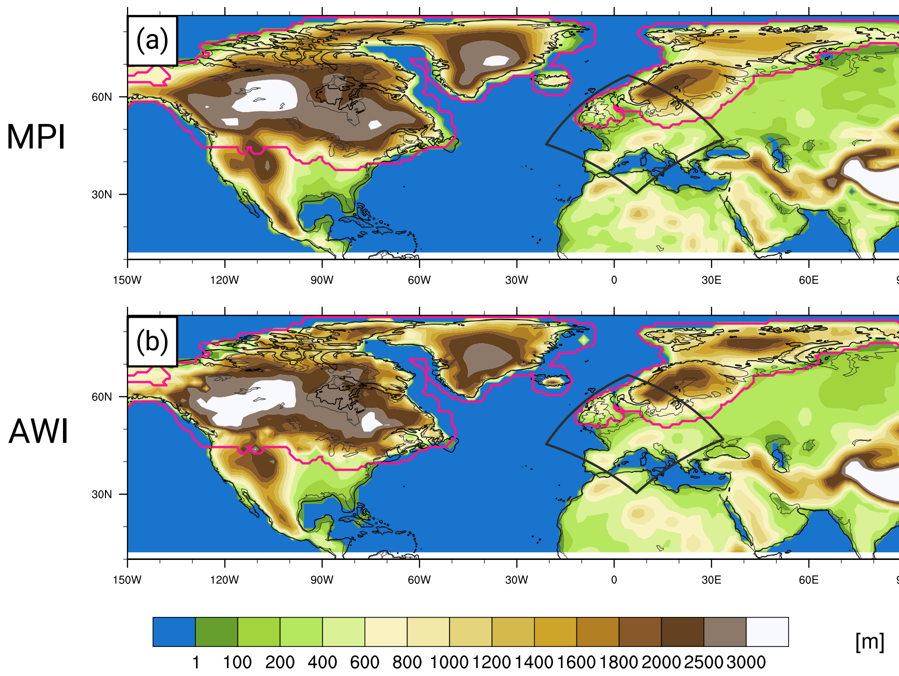

Figure S2. GCM orography of the MPI *(a)* and the AWI simulation *(b)*. Thick black line: WRF Domain 1, thin black line: LGM coastline, pink line: LGM ice sheet.

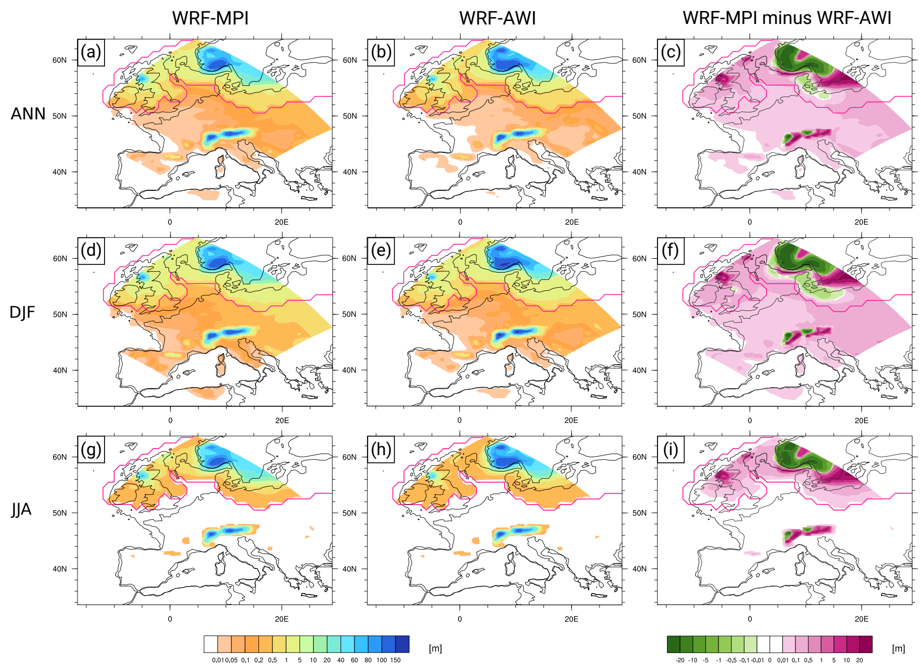

Figure S3. Distribution of snow height in annual *(a-c)* and seasonal winter *(d-f)* and summer *(g-i)* means as simulated with the regional WRF model with MPI forcing *(a*, *d* and *g)* and with AWI forcing *(b*, *e* and *h)* and their differences *(c*, *f* and *i)*. Black line: LGM coastline, pink line: LGM ice sheet.

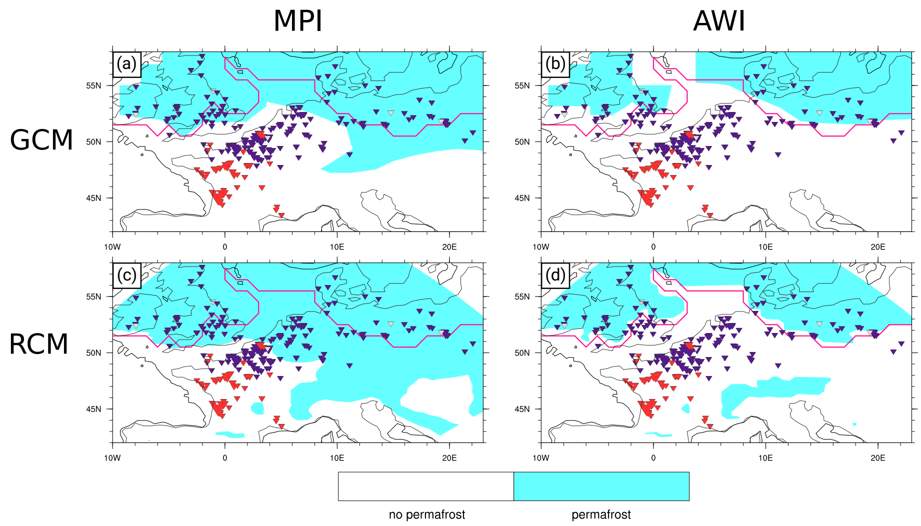

Figure S4. Permafrost distribution based on the annual mean soil temperatures below 0 °C in approximately 70 cm depth as simulated by the global MPI *(a)* and the global AWI simulation *(b)* and their respective regional counterpart *(c* and *d)*. Ice wedge pseudomorphs, composite, and sand wedges from Andrieux et al. (2016) and Isarin et al. (1998) are denoted by purple, grey, and red triangles respectively. Black line: LGM coastline, pink line: LGM ice sheet.

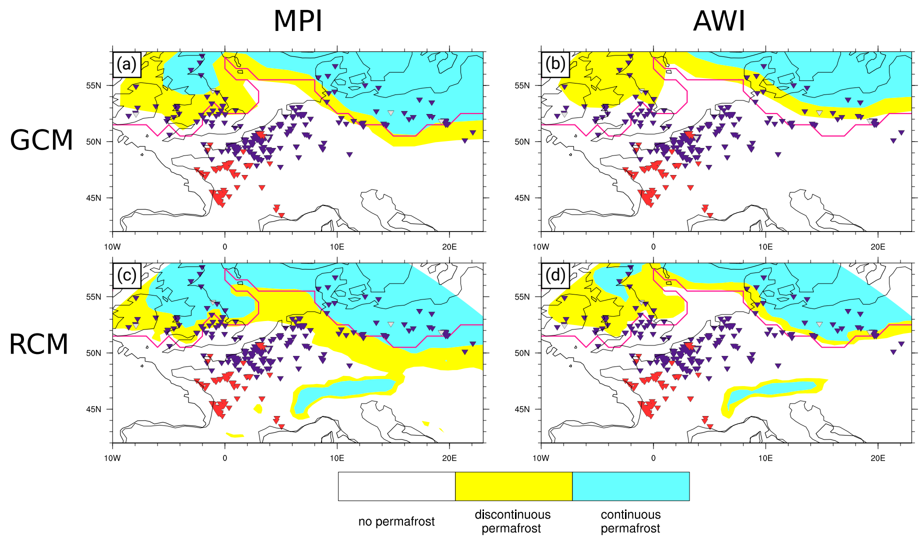

Figure S5. Permafrost distribution based on the mean annual air temperature (MAAT) as simulated by the global MPI *(a)* and the global AWI simulation *(b)* and their respective regional counterpart *(c* and *d)*. Ice-wedge pseudomorphs, composite, and sand wedges from Andrieux et al. (2016) and Isarin et al. (1998) are denoted by purple, grey, and red triangles respectively. Black line: LGM coastline, pink line: LGM ice sheet.

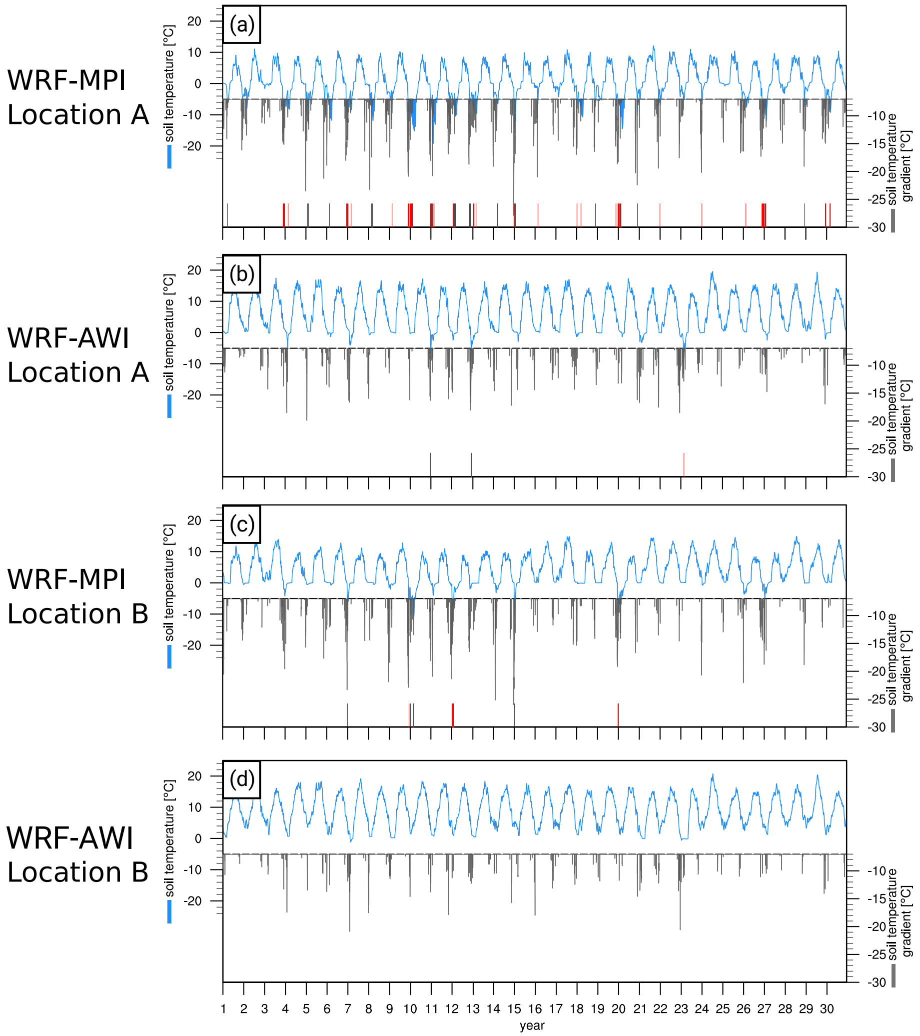

Figure S6. Development of the daily mean soil temperature and soil temperature gradient in location A and B (as denoted in Fig. 1; A: model grid point 49.8° N, 2.49° E; B: model grid point 46.1° N, -0.33° E) as simulated in WRF-MPI *(a* and *c)* and in WRF-AWI *(b* and *d)* for 30 consecutive years. Blue lines show the development of the soil temperatures in layer 3 (70 cm). When the temperatures fall below -5 °C, the first condition for thermal contraction cracking after Matsuoka et al. (2018) is fulfilled, marked with blue shading and the reference line. The soil temperature gradient between the first layer (5 cm depth) and the third layer (grey shading) is only depicted when condition two after Matsuoka et al. (2018) is fulfilled, with a gradient below -7 °C m^{-1}. Red lines indicate the coincidence of the two conditions.

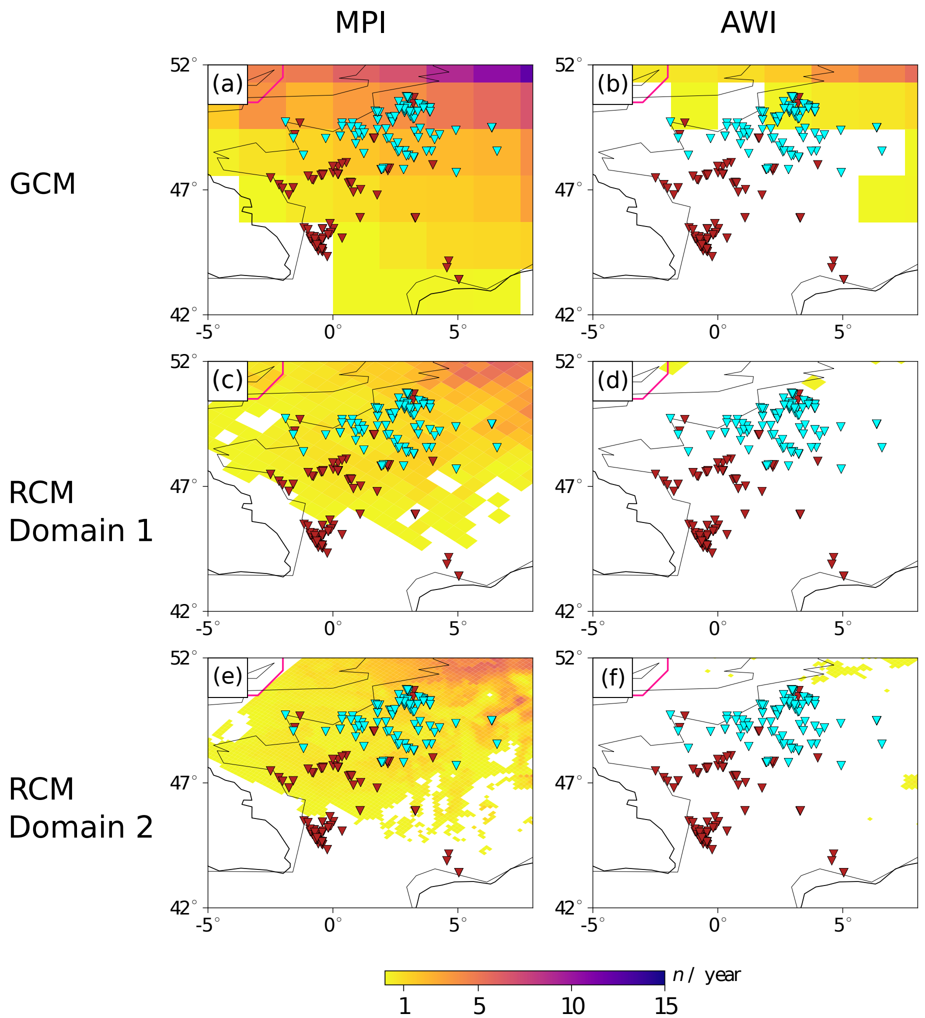

Figure S7. Heat maps of the mean number of days per year when the conditions for deep thermal contraction cracking after Matsuoka et al. (2018) are fulfilled for each grid box in the global MPI *(a)* and AWI simulations *(b)*, and for the first domain of the regional WRF-MPI *(c)* and WRF-AWI *(d)* simulations, as well as for the second domain in WRF-MPI *(e)* and in WRF-AWI *(f)*. Ice wedge pseudomorphs and sand wedges from Andrieux et al. (2016) are highlighted with cyan and red triangles, respectively, only when located in France. Black line: LGM coastline, gray line: LGM ice sheet.